

Effect of surfactants on SrM core-shell nanoparticles synthesised at low temperature

M. Rajesh Kumar¹ ✉, R.Y. Hong^{1,2} ✉

¹College of Chemistry, Chemical Engineering and Material Science, Soochow University, Suzhou 215123, People's Republic of China

²School of Chemical Engineering, Fuzhou University, Fuzhou 350108, People's Republic of China

✉ E-mail: rajeshkumar_vgm@yahoo.com; rhong@suda.edu.cn

Published in Micro & Nano Letters; Received on 8th October 2016; Revised on 5th January 2017; Accepted on 11th January 2017

Different morphology of surfactant capped SrFe₁₂O₁₉ nanoparticles have been synthesised using the co-precipitation method, by adding organic template (oxalic acid) as dispersant during citric acid addition. sodium hexametaphosphate and polyvinyl pyrrolidone used as capping agents. Calcinated surfactant capped SrFe₁₂O₁₉ has been characterised using X-ray diffraction, scanning electron microscopy, transmission electron microscopy, Fourier transform infrared spectroscopy analysis, Raman spectroscopy and vibrating sample magnetometer. The influence of the surfactants on the morphology of SrFe₁₂O₁₉ core-shell nanoparticles was studied.

1. Introduction: Magnetic nanoparticles have been of great interest for researchers in various fields including biomedicine [1, 2]. In biomedicine, magnetic resonance imaging (MRI) is widely used technique to non-invasively see into the human body. Even though MRI has improved diagnostic medicine, there are some problems with it. The size and shape of nanoparticles are important because they will affect certain properties. Iron oxide nanoparticles have been found that a greater half-life than traditional gadolinium-based contrast agents. The optimal size is based on blood half-life rather than magnetic effect. The longer half-life allows for MRI to be used to track blood pooling in a patient. Overall, iron oxide nanoparticles are successful as a contrast agent because their unique size and half-life allows for improved detail in MR images [3]. Even though iron oxide is a good contrast agent, it is harmful to the human body. So, let us move onto M-type hexaferrites. M-type hexaferrite nanoparticles are preferred in medical applications because it is also a contrast agent and harmless to the human body. Size plays an important role while using M-type hexaferrites. In the past, hexaferrites were prepared via hydrolysis reaction, co-precipitation [4], thermal decomposition [5], metal reduction [6], microwave-assisted methods [7] and electrodeposition [8]. However, very small nanoparticles can also result in a low saturation magnetisation or non-specific uptake, which reduces their usefulness. Thus, adequate control of their size and understanding the changes in magnetic properties as a function of nanoparticles size is crucial.

To control the particle size, there is a well known and easy way to introduce surfactants into the sample. By this way, there are too many surfactants available. Sodium hexametaphosphate (SHMP) and polyvinylpyrrolidone (PVP) are the most commonly used surfactants and low cost. These surfactants prevent the nanoparticles from clumping together, ensuring that the particles do not form aggregations.

It is a well-known fact that the coercivity of a particle gradually increases to a maximum value at a particular size, and then rapidly decreases to zero as the particle size further decreases [9]. To improve the properties of SrFe₁₂O₁₉, some measures must be taken such as improving its microstructure, controlling its chemical composition, size and morphology [10]. So, how to prepare the nanoSrFe₁₂O₁₉ with the properties of high purity, ultra-fine, well distributed and excellent magnetic properties has been the focus recently. SrFe₁₂O₁₉ has attracted intensive interests since it was discovered in 1950s for its comprehensive applications in permanent magnets [11], magnetic recordings [12], microwave devices [13]

and so on. The preparation technology of fine SrFe₁₂O₁₉ powder using the citric acid method has been matured [10, 14], and using citric acid the preparation of SrFe₁₂O₁₉ with different morphology has also been reported [15]. However, at low calcination temperature, the preparation of SrFe₁₂O₁₉ with different morphology, excellent magnetic properties using surfactants and organic template has yet not been reported.

2. Experimental section

2.1. Synthesis of surfactant capped SrFe₁₂O₁₉ nanoparticles: For the preparation of surfactant capped SrFe₁₂O₁₉ core-shell nanoparticles, 0.5 g of soluble surfactants (SHMP or PVP) was prepared individually in 50 ml of distilled water using a magnetic stirrer to completely dissolve the contents. About 0.211 g of strontium nitrate [Sr(NO₃)₂] and 4.04 g of Fe(NO₃)₃·9H₂O were dissolved in 50 ml of distilled water in a molar ratio of 1:10. Surfactant was added into Fe(NO₃)₃·9H₂O before adding Sr (NO₃)₂ with continuous stirring. Citric acid was added to the mixture in molar ratio of 1:1 and oxalic acid was added in a mole ratio of 1:8 (Sr²⁺). The pH value of the resultant solution was adjusted to 7 with Na hydroxide. The surfactant capped SrFe₁₂O₁₉ nanoparticles were synthesised. Thus, the resulting nanoparticles were washed several times using distilled water. After washing, the nanoparticles were dried at 80°C. During drying, complete conversion into surfactant capped SrFe₁₂O₁₉ takes place and calcinated using furnace for 2 h at 600°C for PVP and 850°C for SHMP.

3. Results and discussion: The morphology of different samples was analysed by scanning electron microscopy (SEM) and transmission electron microscopy (TEM) technologies. Figs. 1a and b show the SEM images of the sample prepared by adding the surfactant Na hexametaphosphate (SHMP). From Fig. 1a, the morphology is needle-like with the diameter of 10 nm and the length of 1 µm. Fig. 1b shows that the morphology is the formation of flower-like structures from nanorods and resulted in atrophic flowers, which are analogues of a sphere. By the addition of surfactant SHMP, different shaped strontium hexaferrites were obtained. So, the surfactant SHMP is used to obtain different morphology. Figs. 1c and d show the SEM images of sample prepared by adding surfactant PVP. The average particle size of the synthesised strontium hexaferrite with PVP as protective agent was 30 nm after calcination at 600°C for 2 h. Compared with SHMP, PVP capped SrM core-shell nanoparticles are better in case of calcination temperature. PVP

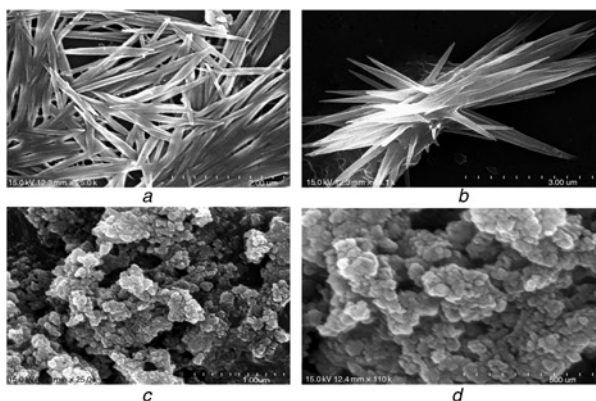


Fig. 1 SEM images of surfactant capped $\text{SrFe}_{12}\text{O}_{19}$ core-shell nanoparticles
a and b SHMP
c and d PVP

has ability to avoid agglomeration because it provides a passive layer on the surface of particles that its electrostatic or steric repulsions would provide stability of the dispersed nanoparticles and prevent the growth or agglomeration of them.

Figs. 2a and b show that TEM images of SHMP capped $\text{SrFe}_{12}\text{O}_{19}$ core-shell nanoparticles. The diameter of nanowires and nanorods around 2 μm . As seen in TEM images, Fig. 2b shows flower-like shape formed by nanorods. In general, SEM (for micrometre resolutions) or TEM (for nanometre resolutions) is used to obtain images of nanostructures. Nanowires and nanorods are very similar, and in most syntheses produced together. The difference lies in the length to diameter ratio of the two. Nanorods are thicker in comparison with nanowires, the latter thus having greater flexibility. However, you cannot see clear distinction between a nanowire and a nanorod by just looking at their SEM and TEM. The real difference lies in their aspect ratios, i.e. the ratio of their length to width of a single nanoentity.

Figs. 2c and d show the TEM images of PVP capped $\text{SrFe}_{12}\text{O}_{19}$ core-shell nanoparticles. As shown in Fig. 2c, the strontium hexaferrite powders have uniform particle size distribution around

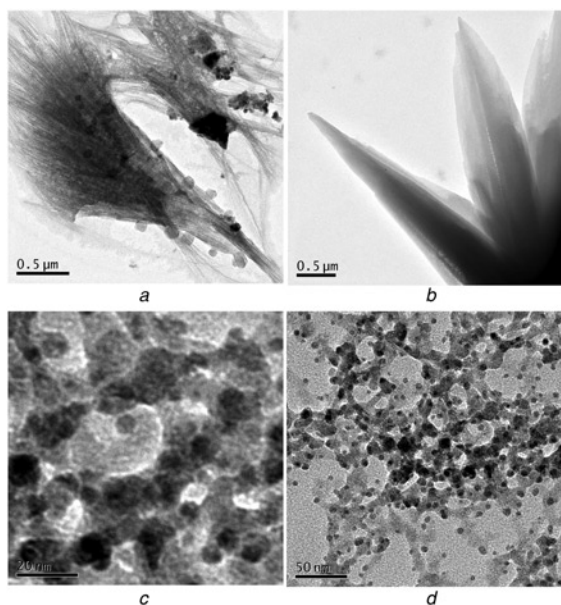


Fig. 2 TEM images of surfactant capped $\text{SrFe}_{12}\text{O}_{19}$ core-shell nanoparticles
a and b SHMP
c and d PVP

Table 1 Comparison of calcination temperature and particles size obtained in the present work and the literature

Method of synthesis	Calcination temperature, $^{\circ}\text{C}$	Particle size D , nm	References
Co-precipitation	600 (PVP)	30	present work
Sol-gel with calcination in Na chloride	790	130×50	Sapoletova <i>et al.</i> [16]
Sol-gel	850	80–100	Nga <i>et al.</i> [17]
Molten-salt-assisted co-precipitation	950	0.8–1.2 μm	Liu <i>et al.</i> [18]

15–30 nm and spherical shape. As shown in Fig. 2d, the strontium hexaferrite powders have narrow particle size distribution of 20–30 nm. From above results, it can be seen that PVP capped strontium hexaferrite powders annealed at 600 $^{\circ}\text{C}$ show good agreement with SEM results.

Table 1 compares the characteristics of $\text{SrFe}_{12}\text{O}_{19}$ powders prepared at optimised synthesis conditions in the present work and in [16–18]. $\text{SrFe}_{12}\text{O}_{19}$ powders prepared by a sol-gel method consist of highly agglomerated particles, so for application purposes additional milling process seems to be necessary. Besides, in comparison with the proposed synthesis method, the co-precipitation method using surfactant is required to reduce the calcination temperature for preparation of strontium hexaferrite phase. Co-precipitation method is the ideal method to prepare smaller size particles and surfactants have the ability to reduce the agglomeration.

X-ray diffraction (XRD) patterns of surfactants capped $\text{SrFe}_{12}\text{O}_{19}$ core-shell nanoparticles are shown in Fig. 3. All the peaks in Fig. 3 have been indexed as the $\text{SrFe}_{12}\text{O}_{19}$ (JCPDS card no. 80-1198) as reported before [19], with no impurity phases, and broadening of the peaks is obvious, indicating significant decreasing of particle size. It was found that single-phase $\text{SrFe}_{12}\text{O}_{19}$ powders can be obtained in the existence of PVP and SHMP surfactants, whereas secondary phase (Fe_3O_4) was not detected at 600 $^{\circ}\text{C}$. These results reveal that the addition of surfactant improves the crystallisation of $\text{SrFe}_{12}\text{O}_{19}$ phase. Comparing with the surfactants PVP and SHMP, PVPs have good crystallisation and moreover magnetic property is more at 600 $^{\circ}\text{C}$. However, SHMPs have that around 850 $^{\circ}\text{C}$.

The Fourier transform infrared spectroscopy (FT-IR) spectra of surfactants capped $\text{SrFe}_{12}\text{O}_{19}$ core-shell nanoparticles as well as samples annealed at 600 and 850 $^{\circ}\text{C}$ are shown in Fig. 4. In all samples, the broad peak around 3400 cm^{-1} region is attributed to the stretching vibration of the O–H group of CA and molecular water. The bands at around 1700 cm^{-1} is assigned to the stretching

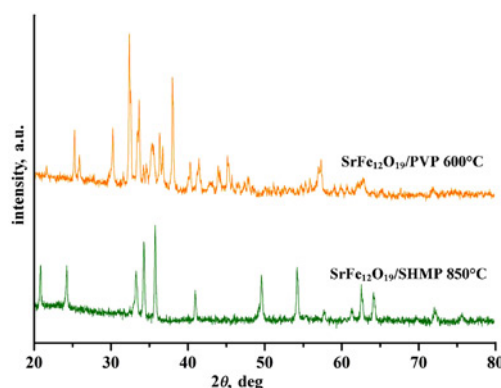


Fig. 3 XRD pattern of surfactants capped $\text{SrFe}_{12}\text{O}_{19}$ core-shell nanoparticles

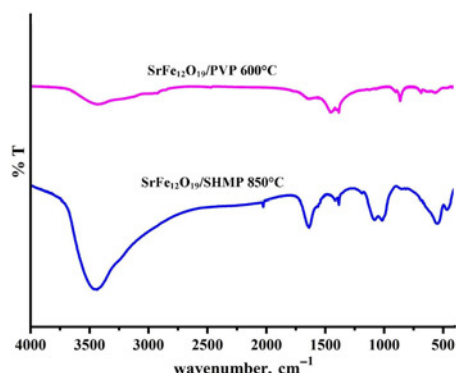


Fig. 4 FT-IR spectra of surfactants capped $\text{SrFe}_{12}\text{O}_{19}$ core-shell nanoparticles

vibrational band of the C=O group of CA. The larger number of IR bending modes ($<800\text{ cm}^{-1}$) observed for PVP capped particles indicates the formation of smaller particles when compared with SHMP capped ones. The sharp peak in PVP capped $\text{SrFe}_{12}\text{O}_{19}$ core-shell nanoparticles around 800 cm^{-1} is the characteristic peaks of PVP, and moreover the doublet peak around $1000\text{--}1200\text{ cm}^{-1}$ is characteristic peaks of SHMP. The broadband around $400\text{--}600\text{ cm}^{-1}$ is attributed to Fe–O bonds. The stretching bands of Fe–O are not visible because of strong overlapping with the bands of $\text{SrFe}_{12}\text{O}_{19}$ at the same wave numbers. Therefore, the bands around 450 and 600 cm^{-1} are characteristic peaks of $\text{SrFe}_{12}\text{O}_{19}$ [20] confirming the presence of hexaferrite phase with them. From the result, it can be inferred that the combustion reaction of the citric acid complex is complete. Thus, formation of $\text{SrFe}_{12}\text{O}_{19}$ phase in the samples heat treated at and above 600°C as concluded from XRD analysis has been confirmed by FT-IR studies.

Raman spectroscopy is an attractive method for studying whether the hexaferrite crystals is substituted or not [21]. Fig. 5 shows that the Raman spectra in room temperature, which further confirm the presence of surfactants capped $\text{SrFe}_{12}\text{O}_{19}$ core-shell nanoparticles and is shown in XRD patterns and TEM images.

The bands in Raman spectra will shift when substitution is occurring. A group theory treatment leads to 42 Raman active modes for $\text{SrFe}_{12}\text{O}_{19}$ ($11A_{1g} + 14E_{1g} + 17E_{2g}$) [22]. There are five important modes of $\text{SrFe}_{12}\text{O}_{19}$ core-shell nanoparticles such as 325, 410, 519, 609 and 680 cm^{-1} in the Raman spectrum [23]. In the present work, there are two modes (519 and 680 cm^{-1}) and four modes (410, 519, 609 and 680 cm^{-1}) where observed in SHMP and PVP capped $\text{SrFe}_{12}\text{O}_{19}$ core-shell nanoparticles as shown in Fig. 5. Owing to the surfactant effect, the modes will be shifted (325 cm^{-1} into 370 cm^{-1}). Finally, we can conclude that the Raman spectrum confirms the presence of surfactants capped $\text{SrFe}_{12}\text{O}_{19}$ core-shell nanoparticles.

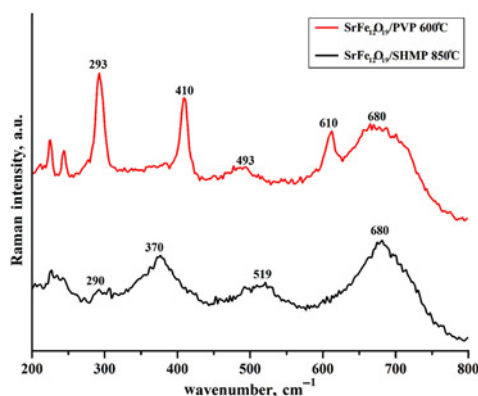


Fig. 5 FT-Raman spectra of surfactants capped $\text{SrFe}_{12}\text{O}_{19}$ core-shell nanoparticles

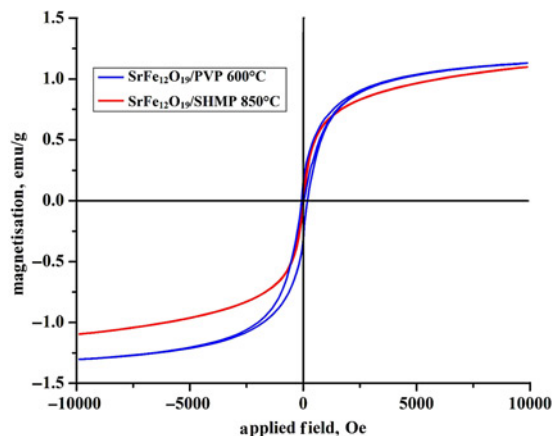


Fig. 6 Magnetisation curve of surfactants capped $\text{SrFe}_{12}\text{O}_{19}$ core-shell nanoparticles

Fig. 6 shows the hysteresis loops obtained from vibrating sample magnetometer using an applied field of $\pm 10\text{ kOe}$ on the surfactant capped $\text{SrFe}_{12}\text{O}_{19}$ particles. As it is well known, the magnetic properties of materials are close relation with their size, morphology, temperature and applied magnetic field. The saturation magnetisation (M_s) of SHMP and PVP capped $\text{SrFe}_{12}\text{O}_{19}$ core-shell nanoparticles are 1.133 and 1.093 emu/g respectively. The remanent magnetisations (M_r) are 0.041 emu/g (SHMP) and 0.345 emu/g (PVP) and the observed coercivities (H_c) are 23.677 Oe (SHMP) and 124.792 Oe (PVP). According to hysteresis loop, PVP capped $\text{SrFe}_{12}\text{O}_{19}$ nanoparticles have a ferromagnetic behaviour [24], whereas SHMP capped $\text{SrFe}_{12}\text{O}_{19}$ nanoparticles have weakly ferromagnetic behaviour.

4. Conclusion: Surfactant capped $\text{SrFe}_{12}\text{O}_{19}$ core-shell nanoparticles were successfully synthesised using the co-precipitation method at low temperature. SEM and TEM images of surfactants capped $\text{SrFe}_{12}\text{O}_{19}$ core-shell nanoparticles showed that the nanoparticles are almost spherical in shape and needle-like shape with homogenous distribution. The synthesised core-shell nanoparticles are homogenous and stable around 30 nm diameter for spherical morphology. FT-IR shows that the presence of surfactants on $\text{SrFe}_{12}\text{O}_{19}$ core-shell nanoparticles surface. Raman spectrum confirms the presence of surfactants capped $\text{SrFe}_{12}\text{O}_{19}$ core-shell nanoparticles. According to hysteresis loop, $\text{SrFe}_{12}\text{O}_{19}$ nanoparticles have a ferromagnetic behaviour for PVP and weakly ferromagnetic behaviour for SHMP. By obtaining surfactant capped $\text{SrFe}_{12}\text{O}_{19}$ core-shell nanoparticles at low temperature, it is very much useful for MRI due to its harmless effect in the human body.

5. Acknowledgments: This work was supported by the National Natural Science Foundation of China (NSFC, grant no. 21246002), the National Post-doctoral Science Foundation, Technology Innovation Foundation of the Ministry of Science and Technology (grant no. 11C26223204581), the Natural Science Foundation of Jiangsu Province (grant no. BK2011328), the 333 Talent project (2013) of Jiangsu Province, the Priority Academic Program Development of Jiangsu Higher Education Institutions (PAPD) and the Minjiang Scholarship of Fujian Province. The authors M. Rajesh Kumar and R.Y. Hong have contributed equally.

6 References

- [1] Lu A.H., Salabas E.L., Schuth F.: 'Magnetic nanoparticles: synthesis, protection, functionalization, and application', *Angew. Chem., Int. Ed.*, 2007, **46**, pp. 1222–1244

- [2] Laurent S., Forge D., Port M., *ET AL.*: 'Magnetic iron oxide nanoparticles: synthesis, stabilization, vectorization, physicochemical characterizations, and biological applications', *Chem. Rev.*, 2008, **108**, pp. 2064–2110
- [3] Kim B.H., Lee N., Kim H., *ET AL.*: 'Large-scale synthesis of uniform and extremely small-sized iron oxide nanoparticles for high-resolution T1 magnetic resonance imaging contrast agents', *J. Am. Chem. Soc.*, 2011, **133**, pp. 12624–12631
- [4] Lee H., Yoon T.-J., Weissleder R.: 'Ultrasensitive detection of bacteria using core-shell nanoparticles and an NMR-filter system', *Angew. Chem., Int. Ed.*, 2009, **48**, pp. 5657–5660
- [5] Zeng H., Li J., Wang Z.L., *ET AL.*: 'Bimagnetic core/shell FePt/Fe₃O₄ nanoparticles', *Nano Lett.*, 2004, **4**, pp. 187–190
- [6] Kim C.W., Kim Y.H., Cha H.G., *ET AL.*: 'A study on the exchange-coupling effect of Nd₂Fe₁₄B/CoFe forming core/shell shape', *Mol. Cryst. Liq. Cryst.*, 2007, **472**, pp. 545–550
- [7] Yamauchi T., Tsukahara Y., Sakata T., *ET AL.*: 'Magnetic Cu–Ni (core-shell) nanoparticles in a one-pot reaction under microwave irradiation', *Nanoscale*, 2010, **2**, pp. 515–523
- [8] Lamichanne M., Rai B.K., Mishra S.R., *ET AL.*: 'Magnetic properties hard-soft SmCo₅–FeNi and SmCo₅–FeCo composites prepared by electroless coating technique', *Open J. Compos. Mater.*, 2012, **2**, pp. 119–124
- [9] Kneller E.F., Luborsky F.E.: 'Particle size dependence of coercivity and remanence of single-domain particles', *Appl. Phys.*, 1963, **34**, pp. 656–658
- [10] Bernier J.C.: 'Chemical processing for electronic ceramics: a challenge', *Mater. Sci. Eng. A*, 1989, **109**, pp. 233–241
- [11] Mozaffari M., Amighian J.: 'Direct use of celestite to prepare presintered SrFe₁₂O₁₉ powders', *Phys. B*, 2002, **321**, pp. 45–47
- [12] Cabanas M.V., Gonzalezcalbet J.M., Valletregi M.: 'Co–Ti substituted hexagonal ferrites for magnetic recording', *J. Solid State Chem.*, 1995, **115**, pp. 347–352
- [13] Zuo X., Shi P., Oliver S.A., *ET AL.*: 'Single crystal hexaferrite phase shifter at Ka band', *J. Appl. Phys.*, 2002, **91**, pp. 7622–7624
- [14] Garcia-Cerda L.A., Rodriguez-Fernandez O.S.: 'Study of SrFe₁₂O₁₉ synthesized by the sol–gel method', *J. Alloys Compd.*, 2004, **369**, pp. 182–184
- [15] Yongfei W., Qiaoling L., Cunrui Z., *ET AL.*: 'Preparation and magnetic properties of different morphology nano-SrFe₁₂O₁₉ particles prepared by sol–gel method', *J. Alloys Compd.*, 2009, **467**, pp. 284–287
- [16] Sapoletova N.A., Kushnir S.E., Li Y.H., *ET AL.*: 'Plate-like SrFe₁₂O₁₉ particles prepared by modified sol–gel method', *J. Magn. Magn. Mater.*, 2015, **389**, pp. 101–105
- [17] Nga T.T.V., Duong N.P., Loan T.T., *ET AL.*: 'Key step in the synthesis of ultrafine strontium ferrite powders (SrFe₁₂O₁₉) by sol–gel method', *J. Alloys Compd.*, 2014, **610**, pp. 630–634
- [18] Liu J.R., Hong R.Y., Feng W.G., *ET AL.*: 'Large-scale production of strontium ferrite by molten-salt-assisted coprecipitation', *Powder Technol.*, 2014, **262**, pp. 142–149
- [19] Danno T., Nakatsuka D., Kusano Y., *ET AL.*: 'Crystal structure of β -Fe₂O₃ and topotactic phase transformation to α -Fe₂O₃', *Cryst. Growth Des.*, 2013, **13**, pp. 770–774
- [20] Jean M., Nachbaur V., Bran J., *ET AL.*: 'Synthesis and characterization of SrFe₁₂O₁₉ powder obtained by hydrothermal process', *J. Alloys Compd.*, 2010, **496**, pp. 306–312
- [21] Kreisel J., Vincent H., Lucazeau G.: 'Raman study of substituted barium ferrite single crystals, BaFe_{12–2x}Me_xCo_xO₁₉ (Me=Ir, Ti)', *J. Raman Spectrosc.*, 1999, **30**, pp. 115–120
- [22] Morel A., Le Breton J.M., Kreisel J., *ET AL.*: 'Sublattice occupation in Sr_{1–x}La_xFe_{12–x}Co_xO₁₉ hexagonal ferrite analyzed by Mössbauer spectrometry and Raman spectroscopy', *J. Magn. Magn. Mater.*, 2002, **242–245**, pp. 1405–1407
- [23] Zhang L., Li Z.: 'Synthesis and characterization of SrFe₁₂O₁₉/CoFe₂O₄ nanocomposites with core-shell structure', *J. Alloys Compd.*, 2009, **469**, pp. 422–426
- [24] Bang J.H., Suslick K.S.: 'Sonochemical synthesis of nanosized hollow hematite', *J. Am. Chem. Soc.*, 2007, **129**, pp. 2242–2243